Probing Structural Perturbation in a Bent Molecular Crystal with Synchrotron Infrared Microspectroscopy and Periodic Density Functional Theory Calculations

Ljupčo Pejov,*,[†] Manas K. Panda,[‡] Taro Moriwaki,[§] and Pance Naumov*,[†]

[†]Institute of Chemistry, Faculty of Natural Sciences and Mathematics, Ss. Cyril and Methodius University, MK−1000 Skopje, Macedonia

[‡]New York University Abu Dhabi, P.O. Box 129188, Abu Dhabi, United Arab Emirates

[§]Japan Synchrotron Radiation Research Institute, 1-1-1 Kouto, Sayo, Hyogo 679-5198, Japan

S *Supporting Information*

ABSTRACT: The range of unit cell orientations generated at the kink of a bent single crystal poses unsurmountable challenges with diffraction analysis and limits the insight into the molecular-scale mechanism of bending. On a plastically bent crystal of hexachlorobenzene, it is demonstrated here that spatially resolved microfocus infrared spectroscopy using synchrotron radiation can be applied in conjunction with periodic density functional theory calculations to predict spectral changes or to extract information on structural changes that occur as a consequence of bending. The approach reproduces well the observed trends, such as the wall effects, and provides estimations of the vibrational shifts, unit cell deformations, and intramolecular parameters. Generally, expansion of the lattice induces red-shift while compression induces larger blue-shift of the characteristic ν(C−C) and ν(C−Cl) modes. Uniform or non-uniform expansion or contraction of the unit cell of 0.1 Å results in shifts of several cm^{-1}, whereas deformation of the cell of 0.5° at the unique angle causes shifts of <0.5 cm^{-1}. Since this approach does not include parameters related to the actual stimulus by which the deformation has been induced, it can be generalized and applied to other mechanically, photochemically, or thermally bent crystals.
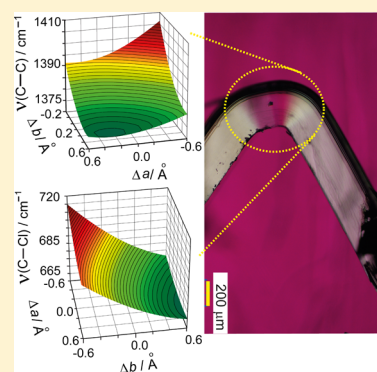
1. INTRODUCTION

When exposed to localized pressure or light, certain organic crystals can bend without fracturing.[1−15] Perhalogenated benzenes such as hexachlorobenzene (HCB, Figure 1), whose crystals can be bent plastically to 360°, which were studied extensively by Reddy and collaborators,[16] are among the first reported examples. More recent studies have brought up additional instances of such mechanically compliant molecular crystals, and at least a dozen of examples of molecular crystals that can bend elastically or plastically when exposed to localized
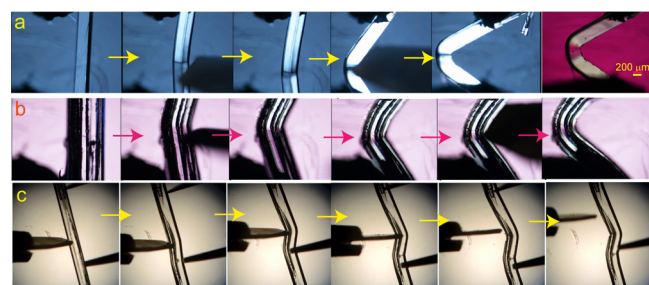

Figure 1. Polarized (a,b) and unpolarized (c) optical micrographs showing mechanically induced plastic bending of hexachlorobenzene crystals.

force in a three-point geometry or to light are now available.[17,18] In our own experience, we have observed the effect with slender crystals from several newly synthesized organic materials which bend readily when poked with a pointy metal object. The original shape of some of the bent crystals can be fully or partially recovered (elastic deformation),[19−22] while others remain permanently deformed (plastic deformation).[23,24] This malleability is counterintuitive for molecular crystals, which are normally considered brittle, and provides one of the most striking demonstrations of the restoring capability of the weak intermolecular interactions that act cooperatively to maintain crystal integrity.[25] Within a broader perspective, these properties bring the ordered molecular solid materials, at least in view of the macroscopic manifestation of their mechanical properties, closer to the mechanically more robust soft materials such as polymers and liquid crystals, and inorganic materials such as metals and alloys.[26−35]

Analysis of the perturbations in a bent crystal, however, remains an intractable problem because the array of lattice orientations that are generated in the bent region of the crystal blurs the diffraction image and results in streaky diffraction profiles. The inaccessibility of the crystal structure at the kink

with diffraction methods has thwarted studies into the atomic-scale perturbations that occur in effect of bending. As a consequence, most of the recent studies on bending crystals have been limited to reports of (oftentimes serendipitous) observations of molecular crystals that can bend under pressure or when exposed to light. Our preliminary results of the attempts to probe the deformation with infrared (IR) spectroscopy are promising;[25] however, interpretation of the spectral signatures of bent crystals could not be accomplished due to complications with the existence of multiple crystal domains that the IR probe encounters on its path through the crystal. Meaningful spectral analysis of a bent crystal requires a computational approach to disentangle the relationships between the local structural perturbations and the intra-molecular vibrations.

Here, periodic density functional theory (DFT) calculations are employed to unravel the effects that individual lattice parameters have on spatially resolved infrared spectra of a bent HCB crystal recorded using infrared microspectroscopy (μIR) with synchrotron radiation. This approach is generally applicable to any bendable single crystal from which IR spectra of sufficient quality can be recorded. It can be applied to obtain perturbations on the atomic-scale structural information that is not accessible with other methods and includes changes in lattice parameters, intermolecular interactions, and bond distances.

2. RESULTS AND DISCUSSION

2.1. Rationale of the Computational Approach. Periodic DFT calculations were performed on the crystal structure of HCB[25] to obtain an exact description of the overall effect of lattice distortions on the wavenumbers of the intramolecular C−C and C−Cl stretching vibrations, $\tilde{\nu}[\nu(\text{C−C})]$ and $\tilde{\nu}[\nu(\text{C−Cl})]$ (for simplicity and in lieu of the common spectroscopic parlance, instead of wavenumber, $\tilde{\nu}$, hereafter the term frequency will be used). For comparison with the experiment, the atomic coordinates were optimized while keeping the unit cell geometry fixed, either at the experimentally determined structure or under conditions of uniform or non-uniform distortion that were introduced by incremental changes in lattice parameters. Uniform distortion was enforced by simultaneous equal (positive or negative) incremental changes in the unit cell axes. Non-uniform distortion was attained by incremental changes of selected unit cell axes (e.g., expansion of a and b while keeping c constant). Full geometry optimization of the atomic coordinates and unit cell parameters was simultaneously performed as a benchmark. Subsequent to the optimization, the harmonic vibrational frequencies at the Γ-point were computed from the dynamic matrix by numerical evaluation of the first derivatives of the analytic atomic gradients. All calculations were carried out with the software CRYS-TAL14[36,37] (Supporting Information).

At the outset, the approach employed here assumes that the vibrational frequency of a particular intramolecular normal mode ν_j can be considered a function of changes in lattice parameters (eq 1),

$$\nu_j = f_j(\Delta a, \Delta b, \Delta c, \Delta \beta) \tag{1}$$

or, alternatively (if more convenient), as a function of the parameters themselves. Provided that the experimental crystal structure is available, the vibrational frequencies can be

computed at a multidimensional grid of points; that is, the frequencies can be treated as a "response surface". At equilibrium geometry, the partial derivatives of frequencies can be calculated as

$$\left(\frac{\partial f_j}{\partial(\Delta a)} \right);\ \left(\frac{\partial f_j}{\partial(\Delta b)} \right);\ \left(\frac{\partial f_j}{\partial(\Delta c)} \right);\ \left(\frac{\partial f_j}{\partial(\Delta \beta)} \right);\ \left(\frac{\partial^2 f_j}{\partial(\Delta a)^2} \right);$$

$$\left(\frac{\partial^2 f_j}{\partial(\Delta \beta)\partial(\Delta a)} \right),\ \text{etc.} \tag{2}$$

and the *changes* in frequencies can be predicted as

$$\Delta \nu_j = \left(\frac{\partial f_j}{\partial(\Delta a)} \right)\Delta a + \left(\frac{\partial f_j}{\partial(\Delta b)} \right)\Delta b + \left(\frac{\partial f_j}{\partial(\Delta c)} \right)\Delta c$$

$$+ \left(\frac{\partial f_j}{\partial(\Delta \beta)} \right)\Delta \beta + \left(\frac{\partial^2 f_j}{\partial(\Delta a)^2} \right)(\Delta a)^2 +$$

$$\cdots + \left(\frac{\partial^2 f_j}{\partial(\Delta a)\partial(\Delta b)} \right)\Delta a \Delta b + \cdots \tag{3}$$

The IR probe passes through macroscopic fractions of the crystal where it encounters microdomains that are deformed to various extents by joint action of compressive and tensile forces. Let q be any combination of geometry parameters within a given segment of the bent crystal, $q = \{a, b, c, \beta\}$. Due to the coexistence of multiple in-crystal segments and the variability of q, the actual (observable) distribution of frequencies of a given mode j due to the distribution of q is

$$g_j(\nu) = \int f_j(\nu, q) p(q)\ \mathrm{d}q \tag{4}$$

In eq 4, $p(q)$ is the normalized probability distribution function that describes the lattice distortion, and $f_j(\nu, q)$ is a function that describes the band-shape of the jth mode at a given structure q (the integration is carried out over all possible values of parameters in the q-space). The vibrational spectrum is a superposition of contributions of all modes at each frequency value ν:

$$S(\nu) = \sum_j g_j(\nu) = \sum_j \int f_j(\nu, q) p(q)\ \mathrm{d}q \tag{5}$$

Therefore, prediction of the spectroscopic features of a bent crystal, or even a semiquantitative explanation of its spectroscopic signature, necessitates two issues to be resolved: (a) the general trends directed by the function $f_j(\nu, q)$, that is, the effect of lattice distortions on the intramolecular frequencies, and (b) distribution of lattice distortions throughout the bent crystal or at least along the path of the incident IR beam. While the former task can, in principle, be accomplished by using modern quantum theoretical methods, the latter is much more challenging and requires experimental information on the structure of the individual crystal segments. However, it is possible to semiquantitatively rationalize the experimental observations by using limited crystallographic information. In the following discussion, these two aspects will be addressed separately. It should be noted that, since the change in crystal geometry q could have a substantial effect on the peak position as well as on the band shape, the crystal

deformation is normally accompanied by band broadening, although the bending could also result in evolution of new bands.

Equations 4 and 5 include the dependence of IR intensity of each particular mode j on the crystal distortion (the departure of the crystal geometry from that of a non-deformed crystal), so that an additional intensity weighing in eq 5 is not necessary. For instance, if the band-shape of the j-th mode of a non-deformed crystal is described by a Gaussian model function:

$$f_j(v, q) = A_j(q) \exp\left[-\frac{(v_j - v_{0j}(q))^2}{2(\sigma_j(q))^2}\right] \quad (6)$$

then the integral intensity of such band is

$$I_j(q) = \int_{-\infty}^{+\infty} f_j(v, q) \, dv = \sqrt{2\pi} A_j(q)\sigma_j(q) \quad (7)$$

In eqs 6 and 7, both the band position (v_{0j}) and the half-width (proportional to σ_j) depend on crystal geometry (q). However, as it is explained below, the periodic DFT calculations indicate that the inherent IR intensity of the vibrational modes—selected for correlation with the structure due to their predictive power—depend only weakly on q.

2.2. Modeling of the Effects of Crystal Deformation on the Infrared Spectra. *2.2.1. Uniform Cell Expansion and Contraction.* We first consider the effects of uniform lattice change on the infrared spectra (Figure 2a). The spectra were sampled as the unit cell was expanded or compressed by concomitant and identical increments of ±0.1 Å along all three axes. The computed frequencies of two pairs of characteristic $v(C{-}C)$ and $v(C{-}Cl)$ modes that are relevant to this study are shown in Figure 2c,d, where the unit cell change is expressed by the change in generalized cell parameter $\Delta p = p - p_0$ (p stands for a, b, or c, and p_0 are the respective values in the non-deformed crystal, taken from the room-temperature crystal structure). The average frequency shifts are summarized in Table 1, and the complete data are deposited as Tables S1–S3, Supporting Information.

The variation of the vibrational frequencies with the generalized lattice parameter p shows that uniform lattice *expansion* induces *red-shift* (lower wavenumbers), while uniform lattice *compression* induces a much larger *blue-shift* (higher wavenumbers) of the $v(C{-}C)$ and $v(C{-}Cl)$ modes (Figure 2c,d). As it is inferred from the insets in Figure 2c,d where the effect is represented as the first derivative $dv/d(\Delta p)$, the steeper slope of the plot when the lattice shrinks relative to the case when it expands implies that the compression exerts a stronger effect on the vibration of these bonds relative to expansion. This result can be rationalized in terms of the Pauli repulsion potentials ("lattice repulsion"), which have a wall-like effect on the respective oscillators. Such wall effects are related to confinement of the atomic motions in the contracted lattice, causing energetically unfavorable electronic overlap between the vibrating motif and the neighbor atoms. In effect, the harmonic force constant of the corresponding oscillator increases as the vibrational potential stiffens, resulting in a blue-shift of the respective frequency. On the contrary, lattice expansion relaxes these effects and accounts for red-shifted frequencies.

The average calculated shifts in the $v(C{-}C)$ and $v(C{-}Cl)$ modes are listed in Table 1 (for uniform deformation, see the "a, b, c" entry). The frequency shifts induced by uniform
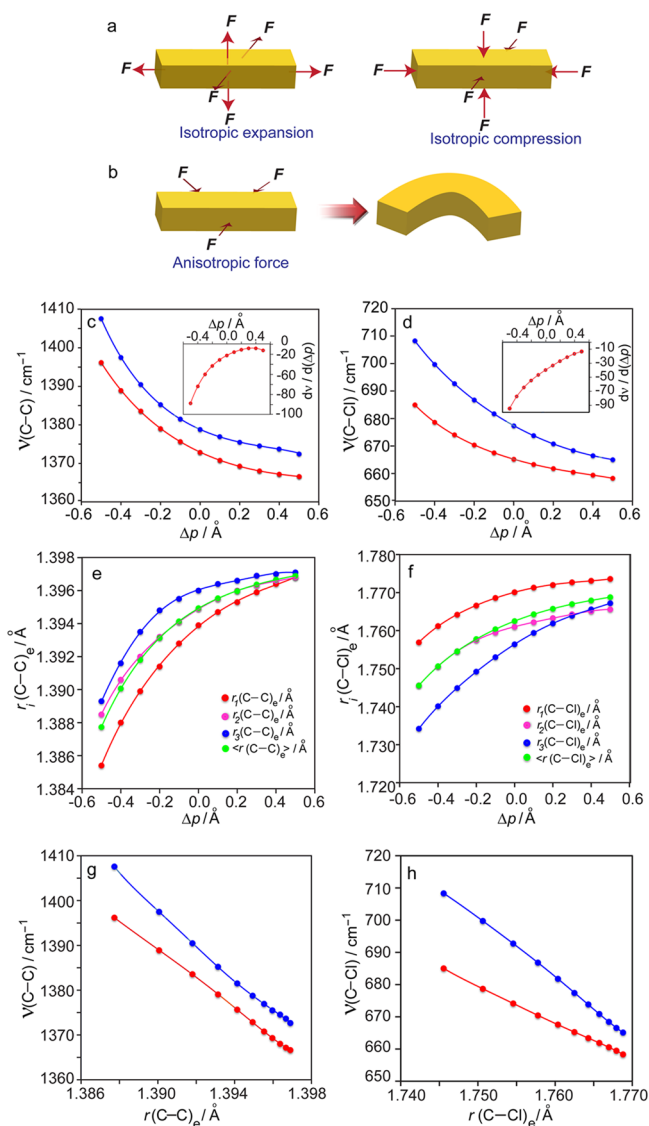

Figure 2. Effect on the vibrational frequencies of uniform changes in the unit cell size of a hexachlorobenzene crystal. (a) Schematic of the uniform expansion and contraction of the unit cell induced by a set of opposing forces (F) whereby the original crystal habit is preserved. (b) Schematic of the effect of non-uniform crystal deformation caused by action of three forces on the unit cell that results in bending of the crystal. (c,d) Dependence of the frequencies of the two selected strong $v(C{-}C)$ (c) and $v(C{-}Cl)$ (d) modes (mode numbers 6 and 22 in Table S1, Supporting Information) on the degree of uniform crystal deformation given as absolute change of the generalized unit cell axis, $\Delta p = p - p_0$, where p stands for a, b or c, and p_0 are the respective values in the non-deformed crystal, taken from the room-temperature crystal structure. The data were fitted with fifth-order polynomial functions (for the actual values of the fitted parameters, see the Supporting Information). The alternative representation in the insets shows the first derivative $dv/d(\Delta p)$ as a function of Δp. (e,f) Dependence on Δp of the intramolecular C–C (e) and C–Cl (f) distances with largest contribution to the relevant normal modes (the average values are given in green color). (g,h) Relation between the wavenumbers of the C–C (g) and C–Cl (h) stretching vibrations and the respective equilibrium distances.

changes in the unit cell which are of the order of the experimentally determined values can be estimated by eq 8:

$$\Delta v = (dv/d(\Delta p))_{\Delta p=0} \Delta p \quad (8)$$

Table 1. Predicted Average Shifts in the Characteristic ν(C−C) and ν(C−Cl) Modes Induced by Expansion/Contraction ($\Delta p = \pm 0.5$ Å) or Distortion ($\Delta\beta = \pm 10°$) of the Unit Cell of a Hexachlorobenzene Single Crystal

| | average wavenumber shift, $\Delta\tilde{\nu}/cm^{-1}$ | | | |
| | ν(C−C) | | ν(C−Cl) | |
	compression	expansion	compression	expansion
a	6.20	0.15	5.88	−1.63
b	11.66	−5.00	12.87	−8.14
c	3.12	−2.40	2.10	−2.09
a, b	20.82	−4.89	21.16	−8.87
b, c	15.41	−6.53	15.38	−9.30
a, c	9.26	−2.82	8.67	−3.37
a, b, c[a]	26.26[a]	−6.43[a]	25.62[a]	−9.90[a]
β[b]	12.66[b]	−0.20[b]	10.08[b]	−1.74[b]

[a]Note that due to ease of calculation, finer grid (0.1 Å) was used in the calculations of the uniform than in the non-uniform (0.5 Å) contraction/expansion. The values shown here were averaged (over four C−C or four C−Cl modes) at deformation of 0.5 Å for direct comparison. More details related to wavenumber shifts at various deformations are given in the Supporting Information. [b]Larger increment ($\pm 10°$) used to calculate the β values was intentionally selected to facilitate comparison with the much larger changes caused by small increments in the unit cell axes. "Expansion" here refers to $\Delta\beta < 0$, while "compression" refers to $\Delta\beta > 0$ ($\Delta\beta = \beta - \beta_0$).

The value of the derivative $d\nu/d(\Delta p)$ calculated at the lattice equilibrium geometry ($\Delta p = 0$) by successive interpolation−differentiation is −22.8 cm^{-1}/Å. For lattice expansion of $\Delta p = +0.1$ Å, eq 8 gives shifts of ~2.3 and 2.4 cm^{-1} for the two ν(C−

C) modes, and ~4.0 and 2.1 cm^{-1} for the two ν(C−Cl) modes (note that the values presented in Table 1 are averaged over all four relevant C−C and C−Cl modes). These values can be used to predict shifts in vibrational frequencies from experimentally determined uniform contraction or expansion of the unit cell where such experiments are possible, for instance, from high-pressure X-ray diffraction analysis.

2.2.2. Non-uniform Cell Expansion and Contraction. We now expand this approach to the case of non-uniform lattice expansion and contraction as a more realistic approximation of the actual lattice deformation in a bent crystal (Figure 2b). A grid of 0.5 Å was used in the calculations. The effect of simultaneous expansion or contraction along two axes on two characteristic vibrational modes, ν(C−C) (mode number 6) and ν(C−Cl) (mode number 22) is shown in Figure 3, and the results are summarized in Table 1 (the "a, b", "b, c" and "a, c" entries) and Tables S4 and S5, Supporting Information.

The overall trends are similar to those observed in case of uniform expansion and compression; unit cell *expansion* results in frequency *red-shifts*, while *compression* causes *blue-shifts*. Due to the wall effect, the contraction has a more pronounced effect on the frequencies of the ν(C−C) and ν(C−Cl) modes relative to expansion. As shown in Figure 3 (panels a, b, g, and h) and Table 1 the frequencies are most significantly affected when the unit cell is simultaneously compressed or dilated along axes *a* and *b*. The crystal structure of HCB (Figure 4) shows that this distortion is related to closest proximity as a result of the most effective packing of the HCB molecules, which maximizes the vibrational confinement. Thus, despite the complexity of the structural changes induced by non-uniform macroscopic crystal deformations, the overall spectral changes of a non-uniformly
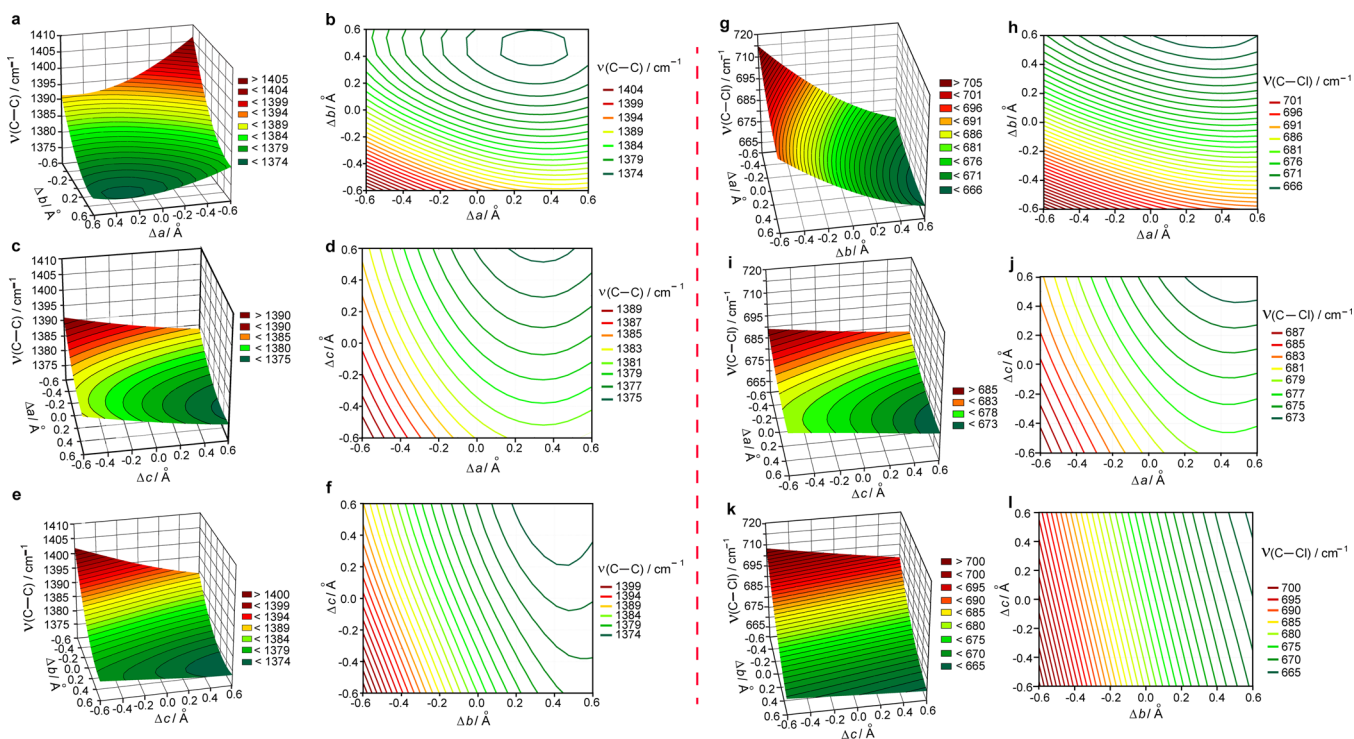

Figure 3. Effect of non-uniform contraction and expansion of the unit cell on the vibrational frequencies of hexachlorobenzene. Two-dimensional cuts through the three-dimensional surfaces are shown together with the respective contour plots. The plots show the effect of changes in the unit cell on selected characteristic modes, ν(C−C) (mode number 6) in panels a−f, and ν(C−Cl) (mode number 22) in panels g−l. Table S1, Supporting Information, contains labeling convention and detailed description of the normal modes. Some of the axes in the 3D plots are shown inverted for clarity of presentation.
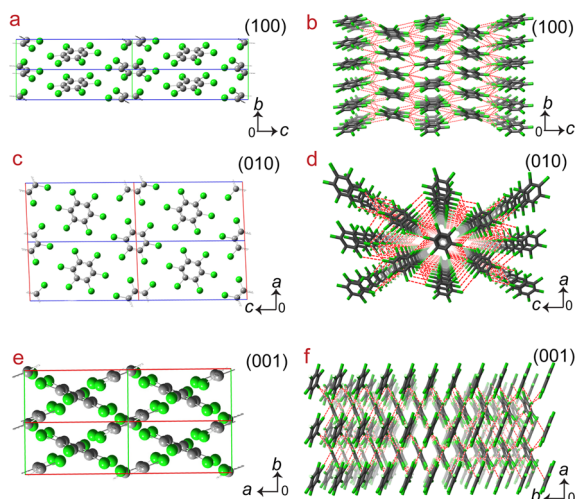
Figure 4. Two-dimensional (a,c,e) and three-dimensional (b,d,f) representations of the molecular packing in a crystal of hexachlorobenzene viewed along the *a* axis (a,b), *b* axis (b,d), and *c* axis (e,f). The red broken lines show the Cl---Cl contacts.

distorted crystal can be rationalized similarly to the uniform compression/expansion. Regardless of its origin, compression is expected to result in frequency upshift. Expansion, on the other hand, causes frequency downshift, however the effect is smaller relative to compression.

To obtain insight into the magnitude of the frequency shifts upon non-uniform crystal deformation, $\Delta\nu$ can be approximated to the first order:

$$\Delta\nu = \left(\frac{\partial\nu(p_1, p_2)}{\partial(p_1)}\right)_{p2=p2,\text{exp.}} \Delta p_1 + \left(\frac{\partial\nu(p_1, p_2)}{\partial(p_2)}\right)_{p1=p1,\text{exp.}} \Delta p_2$$

(9)

Interpolation of the "response surface" of $\Delta\nu$ as a multivariate second-order polynomial in p_1 and p_2 (with a cross-term),

$$\Delta\nu(p_1, p_2) = z_{00} + z_{10}p_1 + z_{01}p_2 + z_{20}p_1^2 + z_{02}p_2^2 + z_{11}p_1p_2$$

(10)

and subsequent calculation of the partial derivatives in eq 9 gives a shift in the overall frequency change of the highest-frequency $\nu(C-C)$ mode of $\sim$−2.0 cm^{-1} when the unit cell simultaneously expands by +0.1 Å along *a* and *b*. Similar results are obtained for the other pairs of variables. Simultaneous expansion by +0.1 Å along *a/c* and *b/c* leads to frequency shifts of this mode of $\sim$−1.3 and −2.3 cm^{-1}, respectively. The corresponding frequency changes of the highest-frequency $\nu(C-Cl)$ mode are −3.6, −1.4, and −3.2 cm^{-1} when the unit cell is simultaneously expanded by +0.1 Å along *a/b*, *a/c*, and *b/c*, respectively. The frequency shifts due to uniaxial expansion/contraction are listed in Table 1 (entries "a", "b" and "c") and Tables S6 and S7 in the Supporting Information.

2.2.3. Unit Cell Distortion. The *distortion* of the unit cell was included in the computations by varying the unique angle (β).
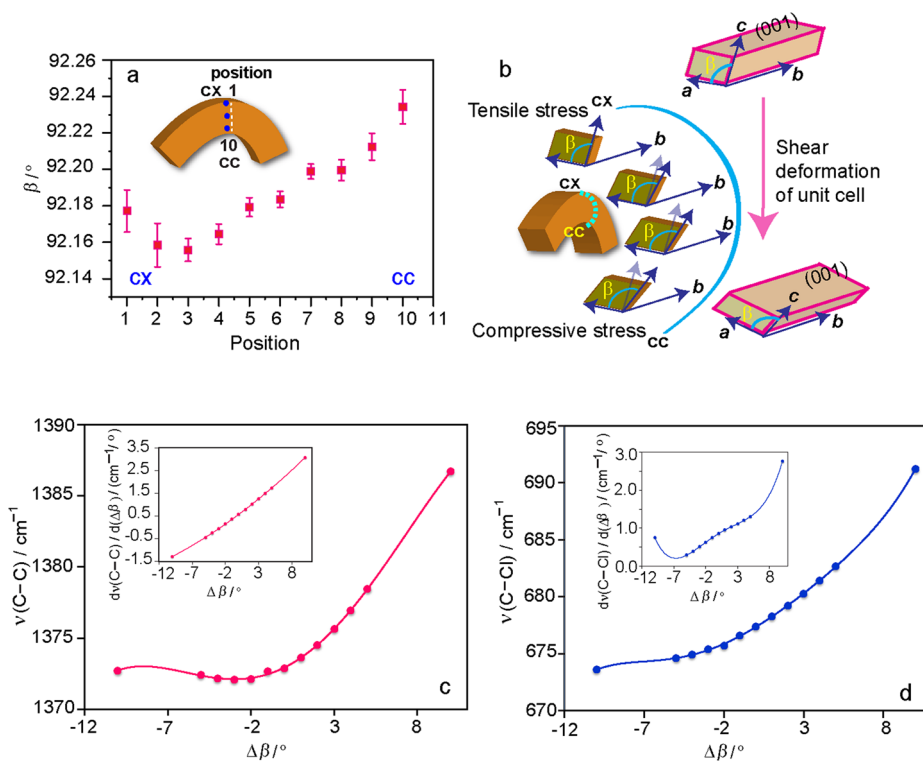

Figure 5. Effect of unit cell distortion, modeled as change in the unique angle β, on the characteristic C−C and C−Cl stretching modes of a hexachlorobenzene crystal. (a) Experimentally observed changes in the unique angle β upon bending (adapted with permission from ref 25, copyright Nature Publishing Group). (b) Cartoon representation of the tensile and compressive forces that develop upon bending on the convex (cx) and concave (cc) side of the crystal, causing deformation of the unit cell and concomitant change in β. (c,d) Dependence of the frequency of characteristic $\nu(C-C)$ (c) and $\nu(C-Cl)$ (d) modes on the unit cell distortion expressed as deformation of β, $\Delta\beta = \beta - \beta_0$, where β_0 is the unique angle in the non-deformed crystal. The insets show plots of the first derivatives of the stretching frequencies with respect to $\Delta\beta$.

Table 1 summarizes the average calculated shifts of the ν(C−C) and ν(C−Cl) modes (the "β" entry) and Tables S8 and S9 in the Supporting Information contain the results. Figure 5c,d shows the relation between the unit cell deformation and the frequencies of two characteristic ν(C−C) and ν(C−Cl) vibrations. The different slopes of the plots are due to the different sensitivity of the two modes on the complex structural perturbations induced by unit cell distortion. Compared to the expansion or compression of the unit cell (changes in only *a*, *b*, and/or *c*), where the relative orientation of the molecules is preserved, the response of the vibrational frequencies to changes in β is related to greater anisotropy, and the analysis is less straightforward. However, the effect on the frequencies is also generally smaller (Table 1). Typically, change in β of +0.5° is expected to cause a frequency shift of only ∼0.3 cm^{-1} for ν(C−C) and ν(C−Cl). The frequency shift induced by change in β of the order of the experimentally determined values[25] can be estimated by

$$\Delta\nu = (d\nu/d(\Delta\beta))_{\Delta\beta=0}\Delta\beta \qquad (11)$$

As a measure of the effect of cell distortion, the derivative $d\nu/d(\Delta\beta)$, computed by successive interpolation-differentiation at the lattice equilibrium geometry ($\Delta\beta = 0$) is +0.6 cm^{-1}/°.

2.3. Analysis of Experimental μIR Spectra. *2.3.1. Assignments in the Spectrum of a Straight Crystal.* Single crystals of HCB bend when the pressure is applied on the (001) face, but break readily when they are pressed on the (100) face. Approximately 12 μm-thick single crystal of HCB was bent in a three-point bending geometry by application of localized pressure on the (001) face and used to record the μIR spectra (Figure 6a−d).[25] The IR probe, cut to size 4 × 8 μm^2, was normal to the bending plane. Figure 6e,f shows the spectral
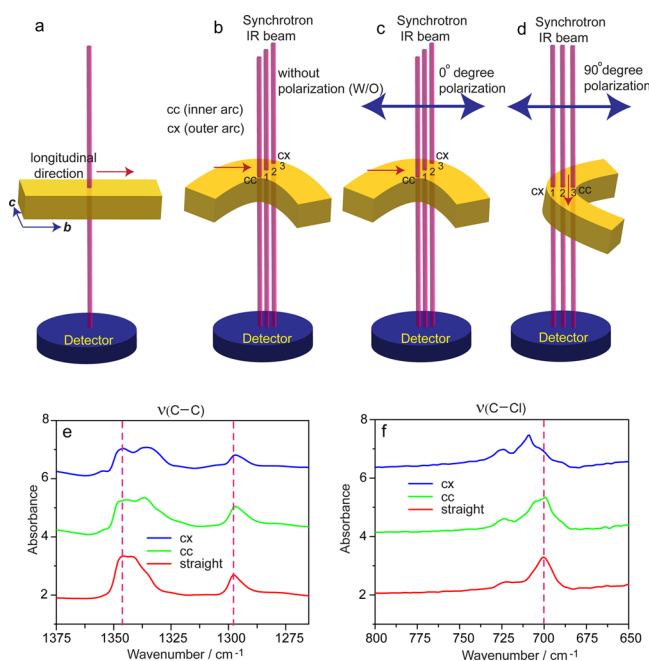

Figure 6. Effect of lattice distortion on the regions of the C−C and C−Cl stretching vibrations in the unpolarized experimental μIR spectra of HCB.[25] (a−d) Sample−instrument geometry used to record the spectra from the straight section (a) and from the convex (cx) and concave (cc) sides of the bent section (b−d) of the bent crystal. (e,f) Effect of bending on the complex bands in the regions of characteristic C−C (e) and C−Cl stretching vibrations.

regions of ν(C−C) and ν(C−Cl) bands recorded from the straight section, and from the convex (cx) and concave (cc) sides of the bent section of the bent crystal. The spectra were analyzed by fitting the complex bands with the smallest number of mixed Gaussian−Cauchy (Lorentzian) bands which provided statistically acceptable fit. The ν(C−C) region of the non-deformed crystal was fitted with 6 bands, at ∼1347, 1342, 1335, 1326, 1298, and 1294 cm^{-1}. The fitted bands are shown in Figure 7, and their assignments are presented in Table 2. The bands in the spectrum of the straight crystal (Figure 7c,f) were assigned[38] based on computational analysis (Table S1, Supporting Information)[39] and comparison with earlier assignments.[40−43]

2.3.2. Assignments in the Spectrum of a Bent Crystal. When a molecular crystal is deformed, a range of segments with varying degree of distortion and various orientation are generated along the path of the IR beam. The IR probe thus samples a set of structures across a continuous range of geometries. As shown in Figure 6e,f, the ν(C−C) bands recorded from the cc and cx sides are significantly broader and have more complex structure relative to the non-deformed part of the crystal. The peak profiles of the bent crystal required more components for satisfactory fitting (Figure 7a,b,d,e). The highest frequency bands on the cc and cx portions of the bent crystal appear at 1354 and 1355 cm^{-1}, respectively, and the lowest-frequency bands are at ∼1294 cm^{-1} in both cases.

While exact assignment of all bands in the spectrum of the bent crystal is not feasible, the origin of some bands can be deduced from their positions and relative intensities. The bands in the 1285−1315 cm^{-1} region (Figure 7a,b) are related to the bands in the 1285−1310 cm^{-1} region of the non-deformed sample. These bands originate from ν(C−C) modes and are of B$_u$ and A$_u$ symmetry, with the B$_u$ bands being stronger (Table S1, Supporting Information). The bands in the 1315−1360 cm^{-1} region correspond to the bands in the same region of the non-deformed crystal. These vibrations are mostly ν(C−C) modes, but they possibly also include contributions from the Kekulé-type ring vibration. In the spectrum recorded from the cx side of the bent crystal, the spectral envelopes in these two regions are notably wider. The bands are clearly red-shifted, and this is especially apparent in the 1360−1315 cm^{-1} region, but also the intensity pattern involves certain redistribution toward higher frequencies (blue-shift). The bands on the cc side are also wider, although they are less red-shifted.

The overlapped ν(C−Cl) bands of the non-deformed crystal form an envelope in the 685−735 cm^{-1} region (Figure 7f). The two strongest bands can be assigned to the ν(C−Cl) modes with B$_u$ symmetry. An additional weaker band due to ν(C−Cl) mode (A$_u$) is also expected in this region. In the bent crystal, these ν(C−Cl) bands are additionally split and overlap in the 685−740 cm^{-1} region (Figure 7d,e). Closer inspection of the relative intensity in the bands of the bent crystal shows tailing on the lower-frequency side in the spectra of the cx and cc sides, and a new band at ∼690 cm^{-1}. Less pronounced tailing to high frequencies is also present in the cx side.

2.3.3. Rationale of the Effects of Bending on the Spectrum. In a real bent crystal the crystal lattice is non-uniformly distorted, and the cumulative effect of the interaction of the IR probe with a variety of geometries on the overall spectrum is best described by the general expression given by eq 5. The probability distribution function is unknown, and thus direct computation of the IR spectrum of the bent sample is not possible. Nevertheless, the expected trends in the
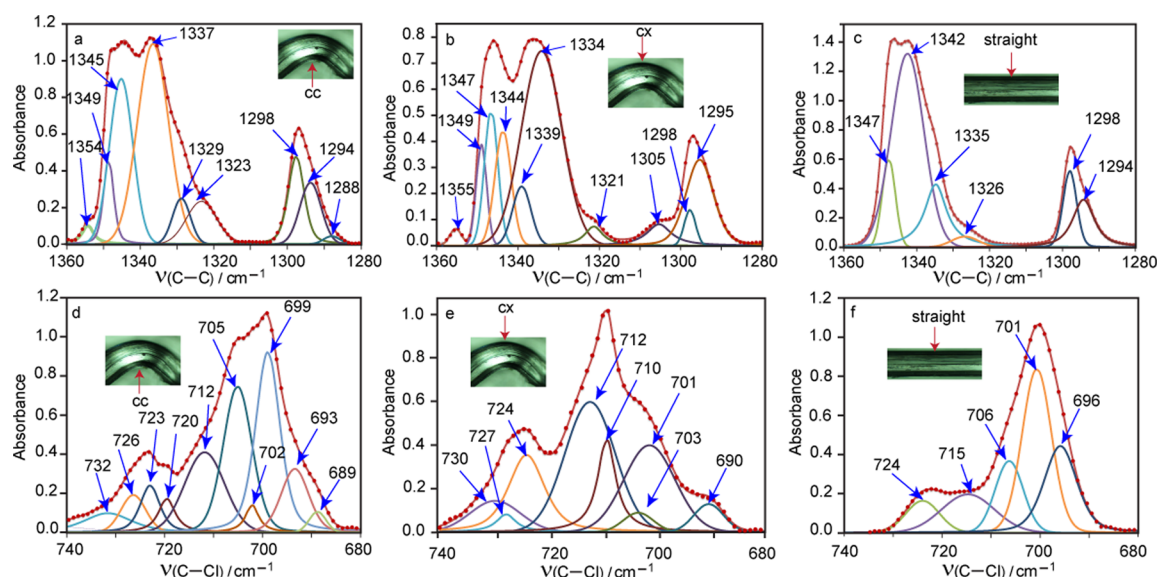
Figure 7. Spectral analysis of the C−C (a−c) and C−Cl (d−f) stretching region of the IR spectra of HCB. The unpolarized spectra recorded from the straight portion of the bent crystal (c,f), and from the concave (cc; a and d) and convex (cx; b and e) sides of the bent section are reconstructed by non-linear fitting with linear combinations of Gaussian and Cauchy (Lorentzian) functions. The numbers are the band wavenumbers in cm^{-1}.

Table 2. Calculated and Experimental (Fitted) Wavenumbers of Selected Characteristic ν(C−C) and ν(C−Cl) Modes, and Assignment Based on Vibrational Analysis and Literature Data

wavenumber, $\tilde{\nu}$/cm^{-1}			
calculated (DFT)[a]	experimental[b]	literature data[c]	assignment (symmetry)[d]
1337.4 (1378.8)	1347.5, 1342.3	1340	ν(C−C) (B$_u$)
1334.8 (1376.1)	1334.9, 1325.9		ν(C−C) (A$_u$)
1331.7 (1372.9)	1297.9, 1293.8	1294	ν(C−C) (B$_u$)
718.0 (677.4)	724.0, 714.7	719	ν(C−Cl) (B$_u$)
706.4 (666.4)			ν(C−Cl) (A$_u$)
705.2 (665.2)	706.3, 700.7	695	ν(C−Cl) (B$_u$)
		695.8	ν(C−Cl) (A$_u$)

[a]Scaled DFT frequencies (the unscaled values are in parentheses). [b]Fitted to the experimentally recorded spectrum (Figure 7). For a complete list of vibrational modes and frequencies see Table S1, Supporting Information. [c]References 40−43. [d]Approximate band description and symmetry.

fundamental modes[44] can be rationalized by accounting for some characteristics of the probability distribution function in special cases, or by comparison with similar systems.

The results can be rationalized with eq 4. In the ideal case of a perfect non-deformed crystal, the probability distribution function $p(q)$ corresponds to a Dirac delta function $\delta(q - q_{straight})$, peaking at the experimental crystal geometry that corresponds to a non-deformed crystal, $q_{straight}$. Subsequent application of eqs 4 and 5 gives the vibrational spectra in the simplest case of a non-deformed crystal:

$$g_j(\nu) = \int f_j(\nu, q)\delta(q - q_{straight})\,dq = f_j(\nu, q_{straight}) \quad (12)$$

$$S(\nu) = \sum_j f_j(\nu, q_{straight}) \quad (13)$$

The function $p(q)$ of a real bent crystal, however, reflects a collection of geometries; thus, the bands in its spectrum are indeed expected to be broader than those of a non-deformed

crystal. The same considerations apply to the ν(C−Cl) bands in Figure 6, where there is even larger band spread to high frequencies (Figure 7d−f). Based on the computational results (see above), this result is attributed to stronger sensitivity of the ν(C−Cl) modes to lattice contraction, which decreases the Cl---Cl and other intermolecular contacts. This results in energetically unfavorable repulsive interactions, and enhances the vibrational confinement effects.

The observed trends in relative intensities are also reflected by the hybrid periodic DFT−integral equation model. While periodic DFT computations predict frequency red-shifts of the ν(C−C) modes upon lattice expansion, the function $p(q)$ that describes the distribution of molecular geometries on the cx side is expected to be asymmetric and to tail toward expanded structures. An opposite trend is expected for the cc side.

2.4. The Inverse Problem: Structural Inferences from Spectroscopic Results. The preceding discussion explains the appearance of the vibrational spectrum of a deformed HCB crystal as a collective result of contributions from individual perturbed lattice parameters. The real value of the spectra−structure correlations, however, is in their predictive power toward changes that occur on a molecular level, in light of the inaccessibility of structural information with diffraction methods. Using vibrational (IR or Raman) spectroscopy to extract structural information represents an "inverse" problem, as inferences on structural parameters are extracted from the spectrum. Although the high molecular symmetry of HCB is in favor of using this system for such purpose, the analysis is complicated by the non-uniform, anisotropic and concomitant changes in the unit cell parameters (a, b, c, and β).

The parameter variation across a range of values can be described by the multidimensional probability distribution function, $p(q)$. Due to the additive properties of the vibrational spectrum given by eq 5, inversion of the full vibrational spectrum is analogous to inversion based on a single-mode band described by eq 4; the inversion of spectroscopic data, most completely described by $p(q)$, is equivalent to finding $p(q)$ from $g_j(\nu)$. Since $p(q)$ is part of the integrand in eq 4, it

may be regarded as Fredholm integral equation of the first kind[45]

$$g(x) = \int_a^b K(x, t)\phi(t)\, dt \tag{14}$$

where the integration is carried out over all possible values of all four structural parameters. In reality, the range of possible values of a, b, c, and β is rather narrow, so $p(q)$ is a peak-shaped function with low dispersion.

$K_j(x,t)$ in eq 14 is the integral kernel. In case of a bent crystal the integral kernel corresponds to the function that describes the band shape of the j-th mode of a non-deformed (straight) crystal, $f_j(\nu,q_{\text{straight}})$. It was already demonstrated above that when one deals with an ideal non-deformed crystal, $g_j(\nu)$ and $f_j(\nu,q_{\text{straight}})$ coincide, because $p(q)$ is a Dirac delta function $\delta(q-q_{\text{straight}})$. Mathematically, in the case when the integral kernel may be written in the form $K(x - t)$ the integral in eq 14 is a convolution of the functions K and ϕ:

$$g(x) = \int_a^b K(x - t)\phi(t)\, dt = K\phi \tag{15}$$

In this specific case, eq 15 can be Fourier-transformed by applying the convolution theorem

$$F[g] = F[K]F[\phi] \tag{16}$$

to obtain the unknown function ϕ by inverse Fourier transformation:

$$\phi = F^{-1}\left[\frac{F[g]}{F[K]}\right] \tag{17}$$

In a general case of the problem treated here, however, the integral kernel does not have to be in difference form, and the integral in eq 4 can be solved numerically.[45] The complexity of the probability distribution function in the bent crystal case and the fact that the integral kernel for each mode contains contributions from several bands allows only semiquantitative analysis of the data. What is actually known is the form of the band-shape function for a given mode j in the case of a non-deformed crystal $f_j(\nu,q_{\text{straight}})$ and the corresponding band-shape function in the case of a deformed crystal, $g_j(\nu)$. The "distortion" of $f_j(\nu,q_{\text{straight}})$ into the observed band $g_j(\nu)$ is modulated by the explicit form of the integral kernel in eq 4, $f_j(\nu, q)$, and by the probability distribution function $p(q)$.

In the experiment, the IR beam encounters deformed unit cells with a range of cell parameters and the probability distribution function provides the most exact description of the deformed crystal structure. Because the deformation is induced externally, the system is not necessarily in equilibrium, and thus the probability distribution is likely a complex function. Nevertheless, conclusions that reflect its asymptotic behavior can be made by considering the theoretical results.

The second factor causing modulation of the band shape of the j-th mode is the integral kernel $f_j(\nu,q)$. It is exceedingly arduous, if not outright impossible, to derive conclusions about the exact form of this function based on experimental data. The dependence of positions of the $\nu(\text{C}-\text{C})$ and $\nu(\text{C}-\text{Cl})$ stretching bands on the crystal deformation were elaborated above in case of simple uniform and non-uniform changes. The crystal is macroscopically distorted, which imposes highly complex and anisotropic unit cell distortions. Assuming simple (Gaussian) shape of the bands corresponding to the selected modes provides a theoretical description of the dependence of

ν_{0j} on q, that is, $\nu_{0j}(q)$ in eq 6. Explicit modeling of the dependence of $\sigma_j(q)$ in eq 6 poses a much more challenging task, because the exact form of the band shape, including its half-width, depends on the dynamics of multiple relaxation processes and their change as the crystal deforms.

The bending of a crystal is occasionally accompanied by evolution of new bands (Figure 7) in the region of the j-th mode that are offset by $\Delta\nu_{0j}$ relative to $\nu_{0j}(q_{\text{straight}})$ (note that in the experimental spectrum the evolution of a new band does not necessarily result in a separate band and could appear as broadening of a band of the non-deformed crystal). The shift in band position is given by

$$\Delta\nu_{0j}(q) = \nu_{0j}(q) - \nu_{0j}(q_{\text{straight}}) \tag{18}$$

and therefore

$$\nu_{0j}(q) = \nu_{0j}(q_{\text{straight}}) + \Delta\nu_{0j}(q) \tag{19}$$

The dependence of ν_{0j} on q can be determined from theoretical calculations. The explicit form of this dependence (a polynomial function) allows us to make the following conclusions. Let us consider an infinitesimal interval dq around q that corresponds to the observed value of ν_{0j} (obtained by simple inversion of theoretical dependencies). The probability distribution function $p(q)$ that appears in the integral equation has a value proportional to the product of the infinitesimal interval $d\nu$ around ν_{0j} and $g_j(\nu_{0j})$. If analyzed in conjunction with the theory, the observed band shape of an arbitrarily deformed crystal provides semiquantitative evidence for the contributions of the structural motifs perturbed within the particular range of q values. For example, appearance of low-frequency bands in the $\nu(\text{C}-\text{C})$ region of a bent crystal or band broadening indicates a range of structures that cause $\nu(\text{C}-\text{C})$ frequency downshift. Likewise, appearance of upshifted $\nu(\text{C}-\text{Cl})$ peaks indicates set of populations in the probability distribution function in which the vibrational confinement causes blue-shift. Deciphering the effects of a particular form of the integral kernel and the probability distribution function on the spectra-structural correlations for individual structural parameters requires experimental spectra of uniformly distorted crystals or of crystals where the effect can be examined by varying each structural parameter independently from the others.

2.5. Comparison with Other Models. An alternative approach to the DFT model described here could be an approach based on the vibrational exciton model similar to the approach of Ostapenko.[46−48] This approach was not directly applicable; if applied to molecular crystals composed of organic molecules that are exposed to highly anisotropic stresses which generate highly anisotropic strain fields, it would lead to exceedingly large number of adjustable parameters. We also note the work of Ordon, Komorowski, and their collaborators on the mechanical perturbation of molecular systems,[49−52] however their work focuses on aspects other than the effect of crystal deformation on the molecular vibrations. Conventional theories of plasticity, on the other hand, as well as their modified variants that explicitly account for the effects related to the length-scale of the material[53−59] are mostly phenomenological and thus they require numerous adjustable parameters which are not in an unequivocal manner related to the molecular parameters relevant to the present study.

3. CONCLUSIONS

The structure perturbations that occur during bending of molecular crystals are not directly accessible with the currently available diffraction methods. On a mechanically bent crystal of hexachlorobenzene (HCB) it is shown here that microfocus infrared spectroscopy with synchrotron radiation can provide semiquantitative information on the changes in the lattice parameters and, provided the crystal structure of the unbent crystal is known, also on the intermolecular distances. The contributions of the distortion of the individual lattice parameters can be deconvoluted by performing a set of calculations on the crystal structure of the unbent crystal within the periodic DFT.

Bending of the HCB crystal is accompanied by frequency shifts and broadening of the intermolecular stretching bands of the unbent crystal, and by evolution of new bands. Generally, lattice expansion results in frequency red-shifts, while contraction brings about stronger blue-shifts. The stronger effect of lattice contraction is ascribed to vibrational wall-like effects.

As a guide to estimate the expected cell distortions, uniform expansion or contraction of the unit cell of 0.1 Å along all three axes results in frequency shift of about 2.3 and 2.4 cm^{-1} in the strongest $\nu(C-C)$ modes and 4.0 and 2.1 cm^{-1} in the strongest $\nu(C-Cl)$ modes. Identical non-uniform expansion or contraction along two unit cell axes results in shift of the $\nu(C-C)$ mode of about 2.0 cm^{-1}. Distortion of the unit cell in respect to the unique angle $\Delta\beta = 1°$ results in shift of about 0.6 cm^{-1}, however the trend in the effect of unit cell distortion on the vibrational frequencies is more complex than the cell expansion/contraction. A model based on the collective contribution of individual unit cell parameters on the probability distribution function is proposed that scrutinizes the effects of bending on the vibrational spectrum.

The approach that we have adopted here—calculation of intramolecular vibrational frequencies in a series of deformed geometries using periodic *ab initio* or DFT methodology—follows the general strategy that has been used in earlier molecular-phenomenological models, such as those that have been developed by Drickamer and Boldyrev.[60−66] However, in contrast to the earlier works which used empirical interatomic interaction potentials to compute the vibrational spectra of crystals under high pressure, the approach described here applies first-principles theory on a non-uniformly deformed (bent) crystal. The approach reproduces well the observed trends, such as the wall effects, and provides estimation of the vibrational shifts, unit cell deformations and intramolecular parameters. Since it generally establishes relations between selected intramolecular vibrational frequencies, unit cell parameters and interatomic distances, it can be generalized and applied to other mechanically or photochemically bent crystals. Considering that the results and the model described here do not include parameters related to the actual stimulus by which the deformation was induced, the approach and the conclusions are generally applicable to molecular crystals that are bent by other external stimuli (light, heat, humidity) provided that high-resolution infrared spectra are available.

4. METHODS

4.1. Infrared Spectra. Commercially available sample of HCB was recrystallized from hexane. As-obtained (unbent) or bent prismatic crystals of size $0.5 \times 0.012 \times 0.010$ mm^3 were used to record the IR spectra. The spectra were recorded by using synchrotron IR radiation at beamline BL43IR of SPring-8 using a Vertex70 spectrometer equipped with a Hyperion 2000 infrared microscope (Bruker). Typically, 2560 spectra at resolution of 2 cm^{-1} were accumulated. Additional details of the experiment are described elsewhere.[25]

4.2. Computations. The quantum mechanical calculations were carried out within the framework of the Kohn−Sham formalism of the DFT. Periodic 3D DFT calculations were carried out by representing the single-particle wave functions (that is, the crystalline orbitals) as linear combinations of Bloch functions, which are defined in terms of local functions (atomic orbitals). The local orbitals were represented as linear combinations of Gaussian type functions. All quantum mechanical calculations were carried out with CRYSTAL14.[36,37] The quantum theoretical methodology in CRYSTAL is based on localized Gaussian-type basis sets. The 6-31G(d) all-electron basis set was used for all carbon atoms. To reduce the computational costs while maintaining sufficiently accurate prediction of the overall trends the large-core version of the Hay-Wadt pseudopotential was adopted to describe the core electrons of the chlorine atoms.[67] The remaining 7 electrons ($3s^2 3p^5$) were described by the two *sp* shells, as described in ref.[68] In a series of test calculations, the pob-TZVP basis of triple-ζ valence with polarization quality developed by Bredow et al.[69] was also used on all C and Cl atoms. In constructing the Kohn−Sham Hamiltonian, a combination of Becke's three-parameter adiabatic connection exchange functional (as implemented in CRYSTAL14 code, i.e., adopting the WVN 5 functional) was used (B3[70]) in combination with the Lee−Yang−Parr (LYP[71]) correlation functional. The application of B3-LYP methodology to study molecular crystals with localized basis sets has been discussed and justified in a number of previous studies,[72−79] although more specialized functionals have been also developed for periodic Hartree−Fock and Kohn−Sham calculations. To control the computation of two-electron Coulomb and exchange integrals as well as the truncation criteria for the infinite sums encountered in the calculations, the following set of TOLINTEG parameters (T1−T5) was used: (7,7,7,7,16). A regular sublattice with shrinking factor of 6 was used to sample the reciprocal space. This corresponds to 80 independent k-points in the irreducible Brillouin zone. For numerical integration in DFT, the pruned grid of 75 radial and 974 angular points (75,974) was used. The suitability of the computational approach was confirmed by comparison of the spectra calculated by periodic DFT with literature data on experimental spectra recorded from an HCB single crystal.[40−43] The periodic DFT computations reproduce remarkably well the experimental single-crystal data (for discussion on the spectral comparison, see the Supporting Information and Table S1 therein). The computational method proved to be robust, and reflects faithfully the non-equilibrium conditions in a strained crystal.

Extensive geometry optimizations were carried out using analytical energy gradients (employing a quasi-Newton optimization scheme, and by updating the second derivative matrix at each energy-computational step by the BFGS algorithm) with respect to the atomic coordinates and in several cases also the unit-cell parameters. To study the effect of (external) crystal deformation on the (intrinsic) structure of the system (the atomic positions within the cell), a series of geometry optimizations were carried out by fixing the lattice parameters at either the experimentally obtained values of *a*, *b*, *c*, and *β*, or at a series of values of these parameters selected so as to emulate both uniform and non-uniform shrinkage/expansion of the crystal (for further details and the actual choice of the grid of points, see the main text and the figures). The criterion for convergence of the SCF Kohn−Sham equations in respect to the total energy was set to 10^{-7}. The convergence during the geometry optimization was controlled by monitoring both gradient component values and the nuclear displacements, using the default criteria in CRYSTAL14. Subsequent to the geometry optimizations, harmonic vibrational analyses were carried out at the Γ-point by computing the dynamical matrix with numerical calculation of the derivatives of the analytically computed atomic gradients. The harmonic vibrational frequencies in the normal-mode approximation were computed by diagonalization of the mass-weighted dynamical matrix. The IR intensities were computed through

the atomic Born effective charge tensors evaluated by the Berry phase methodology.

There are 24 atoms in the unit cell of HCB (2 formula units), leading to 72 vibrational normal modes. Symmetry analysis gives $\Gamma_{total} = 18A_g \oplus 18B_g \oplus 18A_u \oplus 18B_u$. A total of 33 of the modes are IR active, while 36 are Raman active. Additional 3 modes, two of which are of B_u and one of A_u symmetry, correspond to rigid translations. The complete list of normal modes, as well as their frequencies, approximate descriptions and IR intensities are given in Table S1, Supporting Information. The IR-active modes that are the main contributors to the intramolecular C−C and C−Cl stretching vibrations, and have strongest intensities were selected for spectra-structure correlations. In Table S1, Supporting Information, these modes are labeled 6, 8, 22, and 24.

We note that the DFT calculations have been already utilized to support the band assignments in the IR spectra of crystals that were subject to high pressure.[80−84] These studies however used geometry optimizations followed by frequency calculations at a single compressed crystal geometry; a range of deformed geometries that corresponds to bending of a single crystal has not been investigated thus far. The results from the periodic DFT calculations related to the functions $f_j(\nu, q)$ reported here could appear analogous to the case of simple compression of the unit cell, which is expected to result in frequency blue-shifts, or expansion, which leads to red-shifts. On the contrary, the periodic DFT approach applied to a bent crystal accounts for all subtle effects on the frequency of each intramolecular mode that occurs as a result of crystal deformation (for example, altered cooperative effects, dipole−dipole coupling, existence of qualitatively different forces acting on molecules in different directions upon application of anisotropic stresses, etc.). This is brought about the freedom of atomic positions for full relaxation during the PES minimum search at fixed geometry of the deformed unit cell. The existence of a variety of deformations throughout the crystal is accounted for by a suitable function $p(q)$.

◼ ASSOCIATED CONTENT

ⓈSupporting Information

The Supporting Information is available free of charge on the ACS Publications website at DOI: 10.1021/jacs.6b11212.

> Tables S1−S9 with spectroscopic data; complete captions to Figures 2 and 5 (PDF)
> Video 1, crystal bending (AVI)
> Video 2, crystal bending (AVI)
> Video 3, crystal bending (AVI)

◼ AUTHOR INFORMATION

Corresponding Authors
*ljupcop@pmf.ukim.mk
*pance.naumov@nyu.edu
ORCID ⓘ
Manas K. Panda: 0000-0002-6297-2070
Pance Naumov: 0000-0003-2416-6569

Notes
The authors declare no competing financial interest.

◼ ACKNOWLEDGMENTS

◼ REFERENCES

(1) Uchida, E.; Azumi, R.; Norikane, Y. *Nat. Commun.* **2015**, *6*, 7310.
(2) Ragazzon, G.; Baroncini, M.; Silvi, S.; Venturi, M.; Credi, A. *Nat. Nanotechnol.* **2015**, *10*, 70−75.
(3) Kim, T.; Al-Muhanna, M. K.; Al-Suwaidan, S. D.; Al-Kaysi, R. O.; Bardeen, C. J. *Angew. Chem., Int. Ed.* **2013**, *52*, 6889−6893.
(4) Good, J. T.; Burdett, J. J.; Bardeen, C. J. *Small* **2009**, *5*, 2902−2909.
(5) Sun, J.-K.; Li, W.; Chen, C.; Ren, C.-X.; Pan, D.-M.; Zhang, J. *Angew. Chem., Int. Ed.* **2013**, *52*, 6653−6657.
(6) Kim, T.; Zhu, L.; Al-Kaysi, R. O.; Bardeen, C. J. *ChemPhysChem* **2014**, *15*, 400−414.
(7) Zhu, L.; Al-Kaysi, R. O.; Bardeen, C. J. *J. Am. Chem. Soc.* **2011**, *133*, 12569−12575.
(8) Lange, C. W.; Földeaki, M.; Nevodchikov, V. I.; Cherkasov, V. K.; Abakumov, G. A.; Pierpont, C. G. *J. Am. Chem. Soc.* **1992**, *114*, 4220−4222.
(9) Koshima, H.; Ojima, N.; Uchimoto, H. *J. Am. Chem. Soc.* **2009**, *131*, 6890−6891.
(10) Koshima, H.; Ojima, N. *Dyes Pigm.* **2012**, *92*, 798−801.
(11) Bushuyev, O. S.; Singleton, T. A.; Barrett, C. J. *Adv. Mater.* **2013**, *25*, 1796−1800.
(12) Nath, N. K.; Pejov, L.; Nichols, S. M.; Hu, C.; Saleh, N.; Kahr, B.; Naumov, P. *J. Am. Chem. Soc.* **2014**, *136*, 2757−2766.
(13) Chou, C.-M.; Nobusue, S.; Saito, S.; Inoue, D.; Hashizume, D.; Yamaguchi, S. *Chem. Sci.* **2015**, *6*, 2354−2359.
(14) Shtukenberg, A. G.; Punin, Y. O.; Gujral, A.; Kahr, B. *Angew. Chem., Int. Ed.* **2014**, *53*, 672−699.
(15) Cui, X.; Rohl, A. L.; Shtukenberg, A.; Kahr, B. *J. Am. Chem. Soc.* **2013**, *135*, 3395−3398.
(16) Reddy, C. M.; Gundakaram, R. C.; Basavoju, S.; Kirchner, M. T.; Padmanabhan, K. A.; Desiraju, G. R. *Chem. Commun.* **2005**, 3945−3947.
(17) Reddy, C. M.; Kirchner, M. T.; Gundakaram, R. C.; Desiraju, G. R.; Padmanabhan, K. A. *Chem.—Eur. J.* **2006**, *12*, 2222−2234.
(18) Reddy, C. M.; Padmanabhan, K. A.; Desiraju, G. R. *Cryst. Growth Des.* **2006**, *6*, 2720−2731.
(19) Ghosh, S.; Reddy, M. C. *Angew. Chem., Int. Ed.* **2012**, *51*, 10319−10323.
(20) Takamizawa, S.; Miyamoto, Y. *Angew. Chem., Int. Ed.* **2014**, *53*, 6970−6973.
(21) Ghosh, S.; Mishra, M. K.; Kadambi, S. B.; Ramamurty, U.; Desiraju, G. R. *Angew. Chem., Int. Ed.* **2015**, *54*, 2674−2678.
(22) Takamizawa, S.; Takasaki, Y. *Angew. Chem., Int. Ed.* **2015**, *54*, 4815−4817.
(23) Ghosh, S.; Mishra, M. K.; Ganguly, S.; Desiraju, G. R. *J. Am. Chem. Soc.* **2015**, *137*, 9912−9921.
(24) Shishkin, O. V.; Medvediev, V. V.; Zubatyuk, R. I. *CrystEngComm* **2013**, *15*, 160−167.
(25) Panda, M. K.; Ghosh, S.; Yasuda, N.; Moriwaki, T.; Mukherjee, G. D.; Reddy, C. M.; Naumov, P. *Nat. Chem.* **2015**, *7*, 65−72.
(26) Acharya, A.; Bassani, J. L. *J. Mech. Phys. Solids* **2000**, *48*, 1565−1595.
(27) Dunne, F. P. E.; Kiwanuka, R.; Wilkinson, A. J. *Proc. R. Soc. London, Ser. A* **2012**, *468*, 2509−2531.
(28) Patel, J. R. *J. Appl. Phys.* **1958**, *29*, 170−176.
(29) Cottrell, A. H.; Dexter, D. L. *Am. J. Phys.* **1954**, *22*, 242−243.
(30) Kashyap, B. P.; Chaturvedi, M. C. *Mater. Sci. Technol.* **2000**, *16*, 147−155.
(31) Sato, H.; Fujikake, H.; Kikuchi, H.; Kurita, T. *Jpn. J. Appl. Phys.* **2003**, *42*, L476−L478.
(32) Higaki, H.; Takigawa, T.; Urayama, K. *Macromolecules* **2013**, *46*, 5223−5231.
(33) Kamal, T.; Park, S.-Y. *ACS Appl. Mater. Interfaces* **2014**, *6*, 18048−18054.
(34) Sawa, Y.; Urayama, K.; Takigawa, T.; DeSimone, A.; Teresi, L. *Macromolecules* **2010**, *43*, 4362−4369.
(35) Holmes, D. P.; Roche, M.; Sinha, T.; Stone, H. A. *Soft Matter* **2011**, *7*, 5188−5193.

(36) Dovesi, R.; Orlando, R.; Erba, A.; Zicovich-Wilson, C. M.; Civalleri, B.; Casassa, S.; Maschio, L.; Ferrabone, M.; De La Pierre, M.; D'Arco, P.; Noel, Y.; Causa, M.; Rerat, M.; Kirtman, B. *Int. J. Quantum Chem.* **2014**, *114*, 1287−1317.

(37) Dovesi, R.; Saunders, V. R.; Roetti, C.; Orlando, R.; Zicovich-Wilson, C. M.; Pascale, F.; Civalleri, B.; Doll, K.; Harrison, N. M.; Bush, I. J.; D'Arco, P.; Llunell, M.; Causà, M.; Noël, Y. *CRYSTAL14 User's Manual*; University of Torino, 2014.

(38) It should be noted that, for an unbent single crystal, the early literature data provide limited information for definite assignments. The work of Kopelman and Schnepp[40] provides frequencies and descriptive intensities of the bands in the polarized single-crystal IR spectra, without assignment of even the strongest bands. The positions are in excellent agreement with our data (for details, see Table 2). In a much more thorough study by Bates et al.,[41] a detailed analysis of the polarized Raman spectra was reported. Single-crystal IR spectra were analyzed in view of the high-order vibrational transitions (overtones and combination bands).

(39) The assignment of the fundamental spectral bands in the present study is additionally supported by harmonic vibrational analyses from periodic DFT calculations (Table S1, Supporting Information).

(40) Kopelman, R.; Schnepp, O. *J. Chem. Phys.* **1959**, *30*, 597−598.

(41) Bates, J. B.; Thomas, D. M.; Bandy, A.; Lippincott, E. R. *Spectrochim. Acta, Part A* **1971**, *27*, 637−648.

(42) Schnepp, O.; Kopelman, R. *J. Chem. Phys.* **1959**, *30*, 868−873.

(43) Sadakuni, G.; Maehara, M.; Kawano, H.; Nibu, Y.; Shimada, H.; Shimada, R. *Bull. Chem. Soc. Jpn.* **1994**, *67*, 1593−1597.

(44) A more rigorous treatment would normally consider the fact that the actual molecular vibrational potential is anharmonic. The higher-order vibrational transitions experience different dependence on the strain compared to the fundamental modes. Due to the small diagonal anharmonic force constants characteristic for the relevant modes (ν(C−C) and ν(C−Cl)), any mixed-term anharmonic force constant is a higher-order perturbation to the harmonic potential. Therefore, the main trends in the higher-order vibrational transitions are likely to be determined by those in the fundamental transitions.

(45) Kanwal, R. P. *Linear Integral Equations: Theory & Technique*; Springer: Heidelberg, 2013.

(46) Preston, T. C.; Firanescu, G.; Signorell, R. *Phys. Chem. Chem. Phys.* **2010**, *12*, 7924−7933.

(47) Kadashchuk, A.; Ostapenko, N.; Skryshevski, Yu.; Izvekov, S.; Sugakov, V. *J. Lumin.* **1999**, *85*, 113−120.

(48) Kadashchuk, A.; Skryshevskii, Yu.; Vakhnin, A.; Ostapenko, N.; Arkhipov, V. I.; Emelianova, E. V.; Bassler, H. *Phys. Rev. B: Condens. Matter Mater.* **2001**, *63*, 115205-1−115205-10.

(49) Luty, T.; Ordon, P.; Eckhardt, C. J. *J. Chem. Phys.* **2002**, *117*, 1775−1785.

(50) Ordon, P.; Komorowski, L. *Chem. Phys. Lett.* **1998**, *292*, 22−27.

(51) Komorowski, L.; Ordon, P. *J. Mol. Struct.: THEOCHEM* **2003**, *630*, 25−32.

(52) Komorowski, L.; Ordon, P. *Int. J. Quantum Chem.* **2003**, *91*, 398−403.

(53) Christoffersen, J.; Hutchinson, J. W. *J. Mech. Phys. Solids* **1979**, *27*, 465−487.

(54) Aifantis, E. C. *Int. J. Plast.* **1987**, *3*, 211−247.

(55) Wulfinghoff, S.; Böhlke, T. *Proc. R. Soc. London, Ser. A* **2012**, *468*, 2682−2703.

(56) Hart, E. W. *Acta Metall.* **1970**, *18*, 599−610.

(57) Gupta, A.; Steigmann, D. J.; Stölken, J. S. *J. Elast.* **2011**, *104*, 249−266.

(58) Fleck, N. A.; Muller, G. M.; Ashby, M. F.; Hutchinson, J. W. *Acta Metall. Mater.* **1994**, *42*, 475−487.

(59) Fleck, N. A.; Hutchinson, J. W. *J. Mech. Phys. Solids* **1993**, *41*, 1825−1857.

(60) Moon, S. H.; Drickamer, H. G. *J. Chem. Phys.* **1974**, *61*, 48−54.

(61) Fishman, E.; Drickamer, H. G. *J. Chem. Phys.* **1956**, *24*, 548−553.

(62) Benson, A. M.; Drickamer, H. G. *J. Chem. Phys.* **1957**, *27*, 1164−1174.

(63) Edwards, C. M.; Butler, I. S. *Coord. Chem. Rev.* **2000**, *199*, 1−53.

(64) Miller, P. J.; Block, S.; Piermarini, G. J. *J. Phys. Chem.* **1989**, *93*, 462−466.

(65) Boldyrev, V. V. *Solid State Ionics* **1993**, *63−65*, 537−543.

(66) Chupakhin, A. P.; Sidel'nikov, A. A.; Boldyrev, V. V. *React. Solids* **1987**, *3*, 1−19.

(67) Hay, P. J.; Wadt, W. R. *J. Chem. Phys.* **1985**, *82*, 284−298.

(68) Apra, E.; Stefanovich, E.; Dovesi, R.; Roetti, C. *Chem. Phys. Lett.* **1991**, *186*, 329−335.

(69) Peintinger, M. F.; Oliveira, D. V.; Bredow, T. *J. Comput. Chem.* **2013**, *34*, 451−459.

(70) Becke, A. D. *Phys. Rev. A: At., Mol., Opt. Phys.* **1988**, *38*, 3098−3100.

(71) Lee, C.; Yang, W.; Parr, R. G. *Phys. Rev. B: Condens. Matter Mater. Phys.* **1988**, *37*, 785−789.

(72) Vener, M. V.; Shishkina, A. V.; Rykounov, A. A.; Tsirelson, V. G. *J. Phys. Chem. A* **2013**, *117*, 8459−8467.

(73) Vener, M. V.; Manaev, A. V.; Egorova, A. N.; Tsirelson, V. G. *J. Phys. Chem. A* **2007**, *111*, 1155−1162.

(74) Munshi, P.; Guru Row, T. N. *J. Phys. Chem. A* **2005**, *109*, 659−672.

(75) Oddershede, J.; Larsen, S. *J. Phys. Chem. A* **2004**, *108*, 1057−1063.

(76) Hathwar, V. R.; Guru Row, T. N. *J. Phys. Chem. A* **2010**, *114*, 13434−13441.

(77) Hathwar, V. R.; Gonnade, R. G.; Munshi, P.; Bhadbhade, M. M.; Guru Row, T. N. *Cryst. Growth Des.* **2011**, *11*, 1855−1862.

(78) Munshi, P.; Thakur, T. S.; Guru Row, T. N.; Desiraju, G. R. *Acta Crystallogr., Sect. B: Struct. Sci.* **2006**, *62*, 118−127.

(79) Munshi, P.; Guru Row, T. N. *Acta Crystallogr., Sect. B: Struct. Sci.* **2006**, *62*, 612−626.

(80) Abdulla, M.; Refson, K.; Friend, R. H.; Haynes, P. D. *J. Phys.: Condens. Matter* **2015**, *27*, 375402.

(81) Jahn, S.; Wunder, B.; Koch-Müller, M.; Tarrieu, L.; Pöhle, M.; Watenphul, A.; Taran, M. N. *Eur. J. Mineral.* **2012**, *24*, 839−850.

(82) Yan, T.; Wang, K.; Duan, D.; Tan, X.; Liu, B.; Zou, B. *RSC Adv.* **2014**, *4*, 15534−15541.

(83) Monteseguro, V.; Rodriguez-Hernandez, P.; Ortiz, H. M.; Venkatramu, V.; Manjon, F. J.; Jayasankar, C. K.; Lavin, V.; Muñoz, A. *Phys. Chem. Chem. Phys.* **2015**, *17*, 9454−9464.

(84) Koch-Müller, M.; Jahn, S.; Birkholz, N.; Ritter, E.; Schade, U. *Phys. Chem. Miner.* **2016**, *43*, 545−561.